Coupling Quantization Among Control Loops of Parallel Grid-Following and Grid-Forming Inverters

Zhang, Zhe; Xiao, Yi; Ruan, Hao; Yang, Yongheng; Blaabjerg, Frede

Published in:
2024 IEEE Energy Conversion Congress and Exposition, ECCE 2024 - Proceedings

DOI (link to publication from Publisher):
10.1109/ECCE55643.2024.10861680

Publication date:
2024

Document Version
Accepted author manuscript, peer reviewed version

Coupling Quantization among Control Loops of Parallel Grid-Following and Grid-Forming Inverters

Zhe Zhang, Yi Xiao, Hao Ruan and Yongheng Yang*
College of Electrical Engineering
Zhejiang University
Hangzhou, China
eezz@zju.edu.cn, yi_xiao@zju.edu.cn, ruanhao@zju.edu.cn, yoy@zju.edu.cn

Frede Blaabjerg
AAU Energy
Aalborg University
Aalborg, Denmark
fbl@energy.aau.dk

***Abstract*—The application of Grid-forming (GFM) inverter can be an effective way to enhance the stability of the grid-connected inverters in parallel, and it is necessary to evaluate the interaction among hybrid inverters with Grid-following (GFL) and GFM controls. This paper proposes a method to quantitatively analyze the coupling among power loops of hybrid inverters with GFL and GFM controls. By utilizing the dynamic relative gain array (DRGA) theory on the power transfer function matrix, this method analyzes the interactive impact among power loops of multiple inverters. Firstly, the full-order state-space models of the hybrid inverters with GFL and GFM controls are established. Then, the influence of various control parameters and grid strength on the coupling effect is explored with the proposed method. It is demonstrated through the exploration that the line impedance and the GFM inverter have a significant impact on the power interaction in the low-frequency range, while the current-feedforward control reduces the power coupling among GFL and GFM inverters effectively. The effectiveness of the proposed method and the accuracy of the discussions are verified through simulation and experimental tests.**

***Index Terms*—paralleled inverters; coupling analysis; relative gain array; grid-following; grid-forming;**

I. Introduction

With the worldwide application of inverter-based resources (IBR) in the power system, the characteristics of the grid are rapidly changing towards low inertia and insufficient damping, where grid-following (GFL) inverters are commonly used [1]. The GFL inverter is controlled as a current source, and with a large-scale adaptation of GFL inverters, the stability of the entire system is challenged. Accordingly, grid-forming (GFM) control emerges and is applied to improve the system stability margin by providing frequency and voltage support at the point of common coupling (PCC) [2]. Conventionally, the inverter with GFM control is controlled as a voltage source to give the power response to the grid event, e.g., frequency variation and voltage drop. The virtual synchronous generator (VSG) control is a widely-applied GFM technology, which makes the inverter behave like a synchronous generator (SG) by applying the swing equation in the active power control loop and automatic voltage regulator (AVR) in the reactive power control loop, respectively [3], [4].

This work was supported by the National Natural Science Foundation of China through the project 52107212.

In a system with multiple grid-connected inverters, the interaction paths include both interactions within the inverters and interactions between the inverters and the grid, which collectively determine the system's dynamic characteristics and performance [5]–[7]. The coupling effect occurs due to the grid impedance, the overlapping control bandwidth and the crossover of filter bandwidths, which results in a more complex operating characteristic of the system [6] and even hazards the stability and robustness of the system by causing multiple resonant frequencies [8]–[10]. The power interaction between the grid-connected inverters and the grid also increases the total harmonic distortion (THD) of the output current and decreases the power quality [11]. Thus, it is important to understand the coupling effect among the grid-connected inverters and the gird to address the stability issues caused by power interaction [12], which can also provide a perspective to understand the interaction characteristics of the entire system.

The clustering-based model in [13] was proposed to analyze the interaction mechanism among multiple GFL inverters via the influence of common current and interactive current, however, the model mainly considers the interaction of GFL inverters in the medium frequency range. By analyzing the participant pattern of the multiple GFL inverters, [14] introduced an identifiable method to classify the system modes into local and interaction modes based on the state-space model. However, This method is based on the deviation of system eigenvalues and cannot clearly and quantitatively analyze the coupling between the system control loops. Dynamic relative gain array (DRGA) is a commonly used method to investigate the interaction of multiple control loops in a multiple-input-multiple-output (MIMO) system [15]. Based on the DRGA principle, [16] studied the interaction between the current loops of the multiple inverters with the change of the grid impedance and system parameters. [17] analyzed the harmonic characteristic of the multiple grid-connected inverters by applying the DRGA to the impedance model of the system. The DRGA was applied in [18] to accurately evaluate the power and frequency coupling of the droop-based GFM inverters. However, the above studies focused on the coupling among inverters with the same control, e.g., GFL or GFM control. As the installation of grid-connected IBRs continues increasing,

many inverters employing the GFL and GFM control in parallel are further complicating the interactions and coupling, which calls for effective solutions to analyze the complex interaction among those units, especially the power coupling effect with a quantitative approach [19], [20].

This paper thus proposes a DRGA-based method to quantitatively evaluate the coupling effect of the power loops among parallel inverters with distinct control. The effect of the GFM inverter and line impedance on the power interaction is studied, and voltage-forward control has proved to be an effective way to reduce power coupling. It's worth to mention this method is also applicable to evaluate the coupling of other control loops among hybrid inverters, e.g., the voltage-vector controller and the current-vector controller. The analysis results are verified by simulation and experimental tests. The reminders of the papers are organized as follows: the principle of the DRGA is introduced in Section II. A coupling quantitation method is proposed to analyze the power transfer matrix of the hybrid inverters in Section III while considering the variation of the grid impedance and system parameters. The analysis results are verified by simulation and experiment tests in Section IV and Section V is the conclusion.

II. DRGA Theory and Interactive Coefficient Gain

The DRGA is commonly used to investigate the interaction of variables in a multiple-input-multiple-output (MIMO) system with input variables $\boldsymbol{u}$ and output variables $\boldsymbol{y}$ at the selected frequency ω [21]. In modern control theory, the dynamic relative gain λ_{ij} indicates one control loop (input: $u_j \rightarrow$ output: y_i) being affected by other loops at ω, which can be expressed as:

$$\lambda_{ij} = \frac{N_{ij}}{D_{ij}} = \frac{\left[\Delta y_i\left(j\omega\right) \Big/ \Delta u_j\left(j\omega\right)\right]_{\Delta u_k=0, k\neq j}}{\left[\Delta y_i\left(j\omega\right) \Big/ \Delta u_j\left(j\omega\right)\right]_{\Delta y_k=0, k\neq i}} \tag{1}$$

where $\lambda_{ij}\left(j\omega\right)$ is the dynamic relative gain of the selected control loop ($u_j \rightarrow y_i$) at ω. N_{ij} is the complex gain of the selected control loop when the other loops are open-loop, and D_{ij} is the complex gain of the selected control loop when the other loops are controlled as closed-loop.

Then the DRGA of the entire system can be calculated in the Laplace domain as,

$$\mathbf{\Lambda}(\mathbf{s}) = [\lambda_{ij}(s)] = \mathbf{G}\left(s\right) \odot \mathbf{G}^{-\mathrm{T}}\left(s\right) \tag{2}$$

in which $\odot$ is the Hadamard product, $\mathbf{G}\left(s\right)$ is the transfer function of the MIMO system with input $\boldsymbol{u}$ and output $\boldsymbol{y}$, and $\mathbf{\Lambda}(\mathbf{s})$ is the DRGA of the system composed of $\lambda_{ij}(s)$.

At ω, λ_{ij} is a complex value as $\lambda_{ij} = a + jb$. According to the DRGA criteria, the closer λ_{ij} is to $(1, 0)$, the less the interaction between the loop ($u_j \rightarrow y_i$) and other loops. As such, the interactive coefficient gain can be defined as the distance d_{ij} between (a, b) and $(1, 0)$, as depicted in Fig. 1.

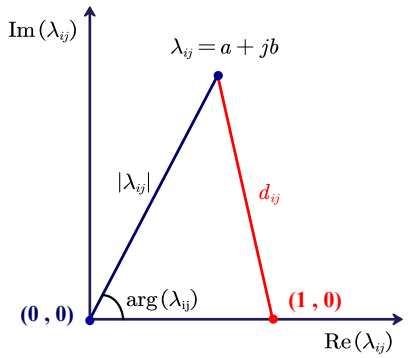

Fig. 1: The relative gain λ_{ij} is located in the the complex plane at ω

This distance d_{ij} quantitatively reflects the coupling degree, and it can be given by:

$$d_{ij} \;=\; |\lambda_{ij}|^2 + 1 - 2\,|\lambda_{ij}|\cos\left(\arg\left(\lambda_{ij}\right)\right) = b^2 + (a-1)^2 \tag{3}$$

with a and b being the real and imaginary part of λ_{ij}, respectively. Therefore, the DRGA $\mathbf{\Lambda}(\mathbf{s})$ can be converted into a real matrix $\mathbf{D}(\mathbf{s})$, being the interactive coefficient array (ICA) of $\mathbf{G}\left(s\right)$. All the elements in $\mathbf{D}(\mathbf{s})$ are non-negative, and d_{ij} has a positive coronation to the coupling degree between the certain control loop ($u_j \rightarrow y_i$) and other loops.

III. Power Interaction Analysis Based on the Proposed Quantization Method

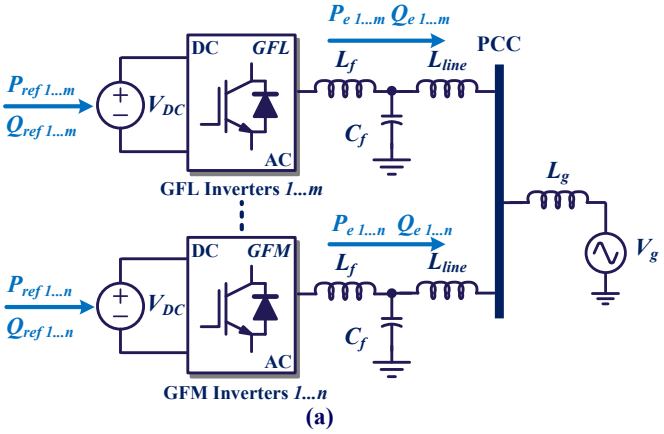

Fig. 2: Configuration of an exemplified system with m GFL inverters and n GFM inverters.

An exemplified system consisting of m GFL inverters and n GFM inverters is depicted in Fig. 2. The GFL inverters employ the PQ-control to inject power (P_e and Q_e) to the grid according to the power command (P_{ref}^{GFL} and Q_{ref}^{GFL}). Similarly, the Virtual synchronous generator (VSG) is adopted as the GFM control with the operating point (P_{ref}^{GFM} and Q_{ref}^{GFM}), and the details of the PQ and VSG control schemes can be found in [1], [5].

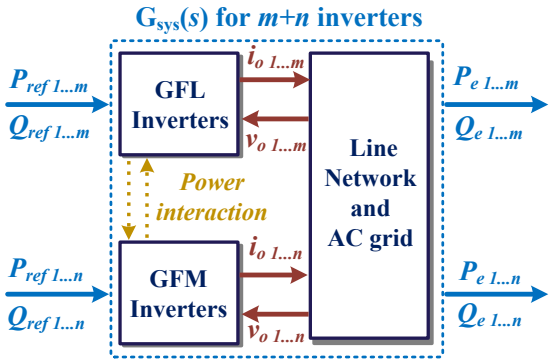

Fig. 3: Open loop MIMO model of an exemplified system with m GFL inverters and n GFM inverters.

A. Modeling of the hybrid inverters

By linearizing the equations of the GFL and GFM control schemes, the small-signal model of the hybrid inverters in parallel can be obtained in a state-space format,

$$\frac{d\boldsymbol{x}}{dt} = \mathbf{A}\boldsymbol{x} + \mathbf{B}\boldsymbol{u}; \lim_{t\to+\infty} \boldsymbol{x} = \boldsymbol{x}_0 \tag{4}$$

with $\boldsymbol{x} \in \mathbb{R}^{l_1}$ being the state variables of the system, $\boldsymbol{u} \in \mathbb{R}^{l_2}$ is the input variables. $\mathbf{A} \in \mathbb{R}^{l_1 \times l_1}$, $\mathbf{B} \in \mathbb{R}^{l_1 \times l_2}$ are the system and input matrix of the system respectively, being the functions of the steady-state vector $\boldsymbol{x}_0$. The dynamic characteristic of the multi-inverter system can be analyzed with matrices $\mathbf{A}$ and $\mathbf{B}$, while the detailed procedures for state-space modeling can be found in [19], [22].

To analyze the power interaction among these inverters, it's needed to analyze the MIMO model of the parallel inverters as shown in Fig. 3, where the power commands (P_{ref} and Q_{ref}) are the inputs $\mathbf{u}$ of the power transfer matrix $\mathbf{G_{sys}}(s)$. The output power (P_e and Q_e) are chosen as the output variables $\mathbf{y}$ and the output matrix $\mathbf{C} \in \mathbb{R}^{2(m+n)\times l_2}$ and $\mathbf{D} \in \mathbb{R}^{2(m+n)\times l_2}$ can be derived by $\boldsymbol{y} = \mathbf{C}\boldsymbol{x} + \mathbf{D}\boldsymbol{u}$. Then $\mathbf{G_{sys}}(s)$ can be obtained,

$$\mathbf{G}_{\text{sys}}(s) = \frac{\boldsymbol{y}(s)}{\boldsymbol{u}(s)} = \mathbf{C}(s\mathbf{I} - \mathbf{A})^{-1}\mathbf{B} + \mathbf{D} \tag{5}$$

Without loss of generality, a hybrid system with a GFL inverter and a GFM inverter in parallel is studied. The circuit parameters and the control parameters of the GFL and GFM inverter are listed in TABLE I and II respectively, while the reactance-resistance ratio (X/R) of all transmission lines is set to 10.

Based on the definition of the ICA in § II, $\mathbf{D}(s)$ of the hybrid inverters (with $m = 1$, $n = 1$) in parallel can be given as,

$$\mathbf{D} = \begin{array}{c} \\ P_e^{GFL} \\ Q_e^{GFL} \\ P_e^{GFM} \\ Q_e^{GFM} \end{array} \begin{array}{c} \begin{array}{cccc} P_{ref}^{GFL} & Q_{ref}^{GFL} & P_{ref}^{GFM} & Q_{ref}^{GFM} \end{array} \\ \begin{bmatrix} d_{11} & d_{12} & d_{13} & d_{14} \\ d_{21} & d_{22} & d_{23} & d_{24} \\ d_{31} & d_{32} & d_{33} & d_{34} \\ d_{41} & d_{42} & d_{43} & d_{44} \end{bmatrix} \end{array} \tag{6}$$

where d_{11} implies the impact of other power loops on the active power loop of the GFL inverter, similarly for other loops, i.e., d_{22} for the reactive power loop of the GFL inverter. d_{33} and d_{44} represent the active and reactive power loops of the GFM inverter respectively. Then, d_{11}, d_{22}, d_{33}, and d_{44} are selected for the following analysis to evaluate the coupling degree among power loops.

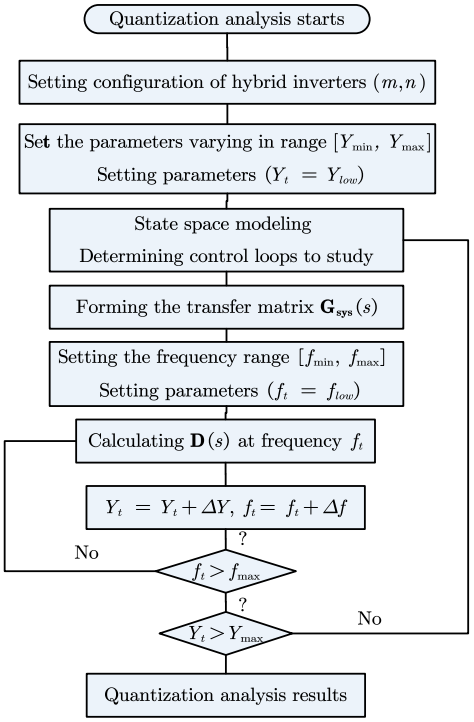

Fig. 4: Flow chart of coupling quantization with the proposed method.

Notably, this method can also be applied to analyze the coupling between any specified control loops ($\mathbf{u} \rightarrow \mathbf{y}$) quantitatively, and the detailed analysis process is illustrated in Fig. 4, which can evaluate the coupling characteristics of desired loops under certain varying parameters Y_t in the frequency range $[f_{min}, f_{max}]$ effectively.

B. Quantitative analysis results of the power interaction

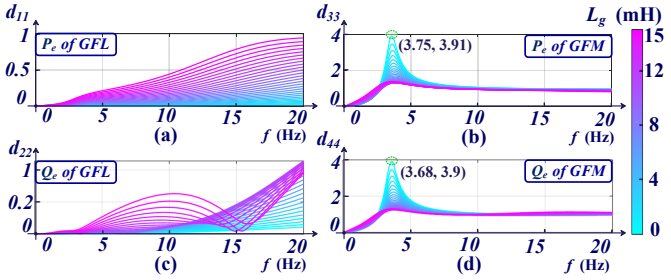

Fig. 5: Quantified coupling effect among power loops with L_g varying in [0, 15] mH. (a) d_{11}, (b) d_{33}, (c) d_{22}, and (d) d_{44}.

For the GFM inverter, the application of VSG inevitably introduces torsional oscillation characteristics of the rotor of

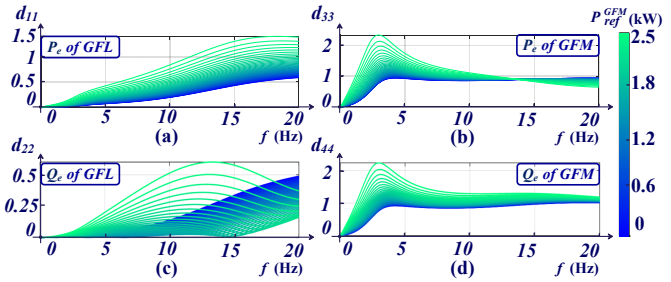

Fig. 6: Quantified coupling among power loops with P_{ref}^{GFM} varying in [0, 2.5] kW. (a) d_{11}, (b) d_{33}, (c) d_{22}, and (d) d_{44}.

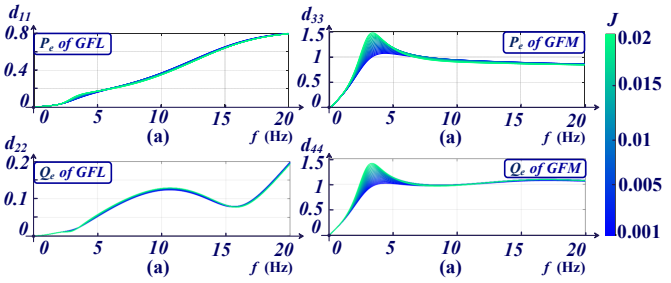

Fig. 7: Quantified coupling among power loops with inertia coefficient J varying in [1e-3, 20e-3]. (a) d_{11}, (b) d_{33}, (c) d_{22}, and (d) d_{44}.

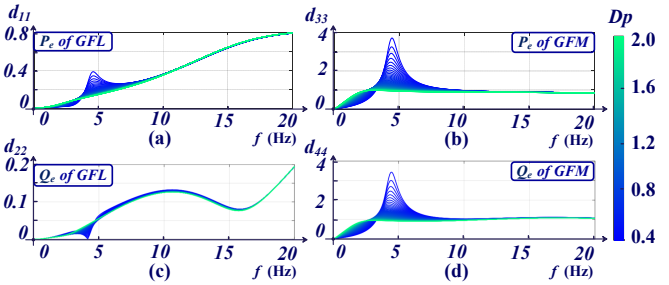

Fig. 8: Quantified coupling among power loops with damping coefficient D_p varying in [0.4, 2]. (a) d_{11}, (b) d_{33}, (c) d_{22}, and (d) d_{44}.

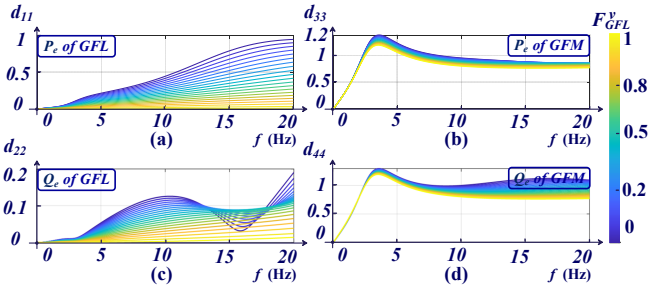

Fig. 9: Quantified coupling among power loops with F_v^{GFL} varying in [0, 1]. (a) d_{11}, (b) d_{33}, (c) d_{22}, and (d) d_{44}.

SG, leading to resonant peaks of the power transfer function of the system in low frequency and affecting the stability of the system [23]. To improve the quality of the output power and meet the specifications of the grid code, the bandwidth of the power loops is required to be set below 10Hz [4] or 5Hz [24]. Thus, the disturbance on the output power is mainly limited within the low frequency, and the power interaction under various grid conditions and control parameters is studied within $[0, 20]$ Hz in this paper.

The impact of the grid impedance L_g on the power interaction is studied with L_g varying in [0, 15] mH. As shown in Fig. 5 (a) and (c), the GFM inverter has a negligible coupling

TABLE I
CIRCUIT PARAMETERS OF THE GRID-CONNECTED INVERTER

Circuit Parameters	Symbol	Value
DC-side voltage	V_{dc}	350 V
AC-side voltage	V_g	110 V
Rated grid frequency	f_0	50 Hz
Switching frequency	f_s	20 kHz
Filter inductance	L_f	4.4 mH
Inductance series resistance	R_f	0.4 Ω
Filter capacitance	C_f	10 μF
Capacitance series resistance	R_d	1 Ω
Transmission line impedance (for GFL)	L_{line}^{GFL}	2 mH
Transmission line impedance (for GFM)	L_{line}^{GFM}	5 mH
Rated active power (for GFL)	P_N^{GFL}	1.5 kW
Rated active power (for GFM)	P_N^{GFM}	2.0 kW
Grid impedance	L_g	15 mH

on the power control loops, when the grid is relatively strong. The mechanism can be explained as a strong grid stabilizing the PCC's voltage, V_{PCC}, against the disturbances from the GFM inverter. As shown in Fig. 5 (b) and (d), with the increase of L_g, the coupling degree between the GFL inverter and the GFM inverter gradually deepens, as the stiffness of V_{PCC} decreases. Conversely, P_e^{GFM} interacting with other power loops gradually decreases with the increase of L_g, which also applies to the Q_e^{GFM} similarly. Considering the relatively weak Interrelation between the GFL inverters and the GFM inverter with a strong grid, the power coupling occurs mainly through the interaction within the GFM inverter (P_e^{GFM} and Q_e^{GFM}), which results similar changing trend for d_{33} and d_{44}. It's also worth noting the coupling peak occurs at 3.75 Hz for the GFM inverter with a strong grid, which indicates P_e^{GFM} and Q_e^{GFM} are more sensitive to the disturbance with a frequency of 3.75 Hz. This quantified coupling peak is verified by the subsequent experimental tests.

Fig. 6 quantitatively analyszes the power coupling under a weak grid (L_g = 15 mH), while the power command of the GFM inverter P_{ref}^{GFM} changes from 0 kW to 2.5 kW. The stiffness of V_{PCC} is weakened under a weak grid condition, and V_{PCC} is more prone to the output power of the GFM inverter. Therefore, with the increase in the output power from the GFM inverter, the interaction of P_e^{GFL}, P_e^{GFM} and Q_e^{GFM} with other loops gradually becomes stronger in the low-frequency range, as shown in Fig. 6 (a), (b) and (d). It's interesting to note that the coupling of Q_e^{GFL} with other loops can be reduced effectively with a proper P_{ref}^{GFM}, as depicted in Fig. 6 (c).

As shown in Fig. 7 (a) and (c), the power coupling between the GFL and the GFM inverter is nearly unaffected by the

TABLE II
CONTROL PARAMETERS OF THE GRID-CONNECTED INVERTER

Circuit Parameters	Symbol	*Value*
GFL control parameters		
Proportional coefficient of the current controller	k_{i_p}	3
Integral coefficient of the current controller	k_{i_i}	800
Voltage-feedforward coefficient	F_v^{GFL}	0
Proportional coefficient of the PLL	k_{pll_p}	0.3029
Integral coefficient of the PLL	k_{pll_c}	0.1345
GFM control parameters		
Inertia coefficient	J	0.01
P-f droop coefficient	D_p	0.944
Q-V droop coefficient	D_q	48.2
Integral coefficient of the Q-V loop	K_Q	0.8
Proportional coefficient of the voltage controller	k_{v_p}	0.085
Integral coefficient of the voltage controller	k_{v_i}	0.15
Voltage-feedforward coefficient	F_v^{GFM}	0
Proportional coefficient of the current controller	k_{i_p}	25
Integral coefficient of the current controller	k_{i_i}	800
Current-feedforward coefficient	F_i^{GFM}	0

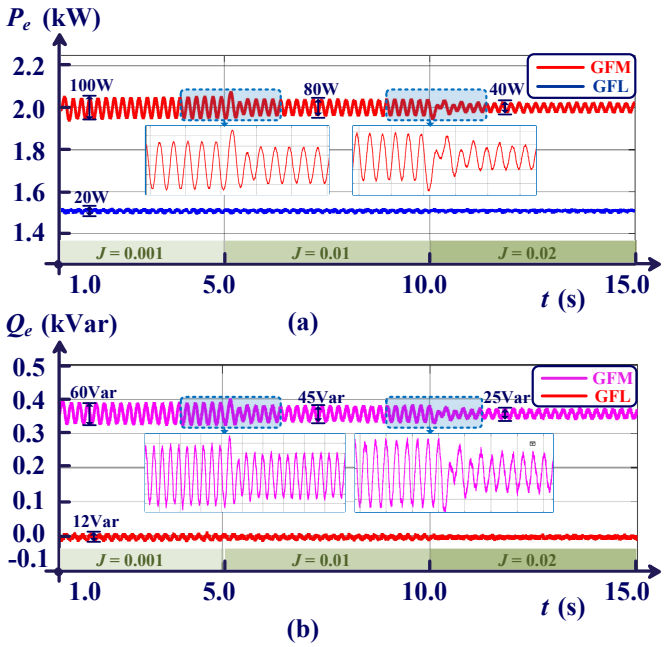

Fig. 10: The output power of the hybrid inverters under disturbance on P_{ref}^{GFM} with J = 2e-3, 1e-2, and 2e-2 respectively, and f_d = 5Hz. (a) P_e^{GFL} and P_e^{GFM}, (b) Q_e^{GFL} and Q_e^{GFM}.

inertia coefficient J varying in [1e-3, 20e-3] in the low-frequency range. The change of J mainly influences the coupling characteristics of the active and reactive power of the GFM inverter, by affecting the frequency and magnitude of the coupling peak around 3.75 Hz. Similarly, the coupling analysis results with the damping coefficient D_p varying in [0.4, 2.0] is illustrated in Fig. 8. The insufficient damping of the GFM inverter introduces the coupling peak of P_e^{GFM} and Q_e^{GFM}, which hazards the robustness of the system. With the increase of D_p, the interaction between P_e^{GFL} with other loops also intensifies, while it has the opposite effect on Q_e^{GFL}.

To improve the GFL inverter disturbance resilience under a weak grid (L_g = 15 mH), a voltage-feedforward term is added with the feedforward gain being F_{GFL}^v, which introduces V_{PCC} to the current-vector controller of the GFL inverter. F_{GFL}^v can significantly reduce the coupling between the GFL inverter and the GFM inverter, as shown in Fig. 9. With F_{GFL}^v changing from 0 to 1, the power interaction of the GFL inverter and the GFM inverter can be suppressed effectively. While F_{GFL}^v is equal to 1, the P_e^{GFL} and Q_e^{GFL} are hardly influenced by other power loops, and the remaining d_{33} and d_{44} indicates the power coupling of the active and reactive power of the GFM inverter.

Based on the above analysis, the power coupling among the hybrid inverters can be concluded as:

1) For the GFM inverter, the power interaction is mainly influenced by the coupling of its own active and reactive power, especially under the strong grid. J and D_p have a significant influence on the interaction of P_e^{GFM} and Q_e^{GFM}, but they have little effect on the output power of the GFL inverter.
2) For the GFL inverter, system configuration including L_g, P_{ref} and Q_{ref} have a strong effect on its coupling characteristics, and it is relatively less influenced by the control parameters of the GFM inverter.
3) Therefore, enhancing the stability of the GFL inverter against the disturbance from the GFM inverter can be achieved by proper system configurations. Stability can also be improved by modifying the control schemes of the inverters, e.g., implementing $P-Q$ decoupling control for the GFM inverter and voltage-feedforward control for the GFL inverter.

IV. SIMULATION AND EXPERIMENT VERIFICATION

A. Simulation Results

To verify the validity of the proposed method, a sinusoidal disturbance with the amplitude of 100 W (5% of P_{ref}^{GFM}) and frequency of 5 Hz is added on the active power command of the GFM inverter, and the circuit and control parameters are set as same as the TABLE I and II.

As shown in Fig. 10, with the increase of inertia coefficient J from 2e-3 to 1e-2 to 2e-2, the active and reactive power of the GFM inverter is less affected by external disturbances. The amplitudes of the 5Hz responses generated by disturbances for P_e^{GFM} decrease, from 100 W to 80 W and further to 40 W. Similarly, the response of Q_e^{GFM} also decrease, which indicates the power interaction between P_e^{GFM} and Q_e^{GFM} attenuates with the increase of the inertia of the GFM inverter, and it is consistent with the analysis in Fig. 7 (a) and (c). The simulation results also indicate that changes in J don't affect the coupling relationship between the GFL and the GFM inverter, and the response amplitude of P_e^{GFL} and Q_e^{GFL} to external disturbances remains nearly unchanged.

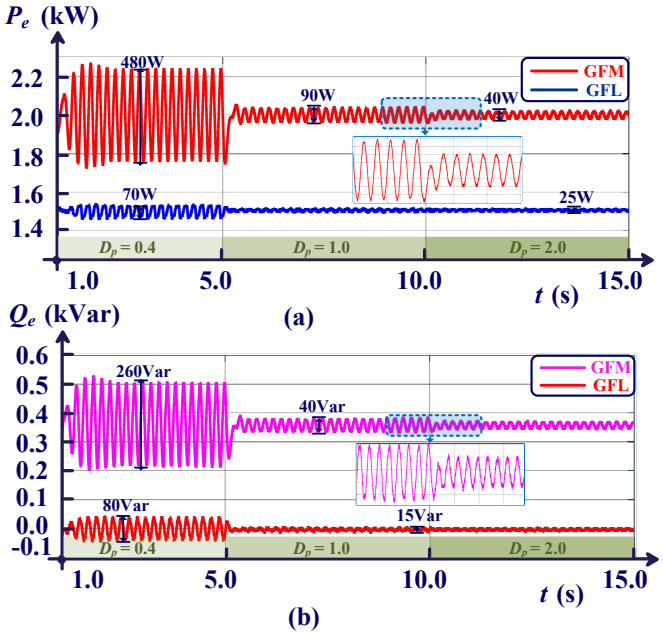

Fig. 11: The output power of the hybrid inverters under disturbance on P_{ref}^{GFM} with D_p = 0.4, 1.0, and 2.0 respectively, and f_d = 5Hz. (a) P_e^{GFL} and P_e^{GFM}, (b) Q_e^{GFL} and Q_e^{GFM}.

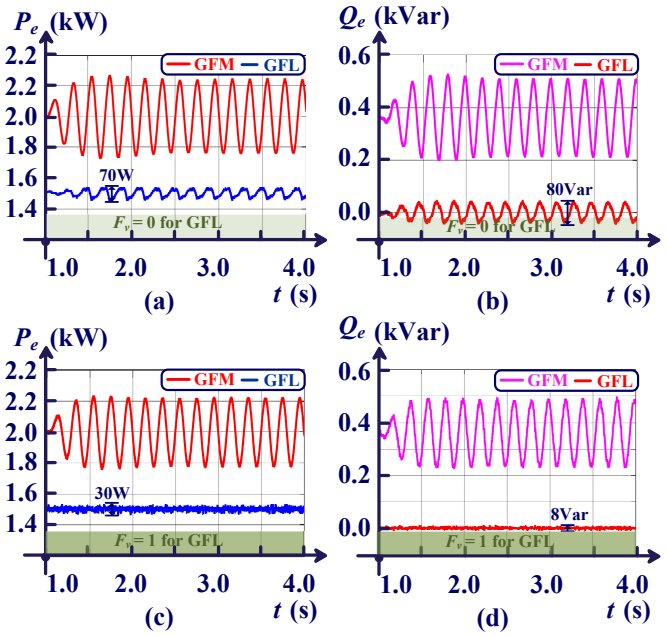

Fig. 12: The output power of the hybrid inverters under disturbance on P_{ref}^{GFM} with F_v = 0 and 1.0 respectively, and f_d = 5Hz. (a) P_e^{GFL} and P_e^{GFM} with F_v = 0, (b) Q_e^{GFL} and Q_e^{GFM} with F_v = 0, (c) P_e^{GFL} and P_e^{GFM} with F_v = 1, (d) Q_e^{GFL} and Q_e^{GFM} with F_v = 1.

Underdamped characteristics of the GFM inverter significantly affect the coupling degree between P_e^{GFM} and Q_e^{GFM}, as shown in Fig. 12. When D_p is equal to 0.4, the response amplitudes of P_e^{GFM} and Q_e^{GFM} to external disturbances can reach 480 W and 260 Var, respectively. It indicates that the system exhibits positive gain for external disturbances, resulting in low robustness to low-frequency disturbances. With the increase of D_p from 0.4 to 1.0 to 2.0, the power response of the GFL inverter and the GFM inverter are both suppressed. Compared with the output power of the GFL inverter, the variation of D_p has a more significant impact on the output power of the GFM inverter, which is in line with the analysis results from the previous section.

For the GFL inverter, the application of the voltage-feedforward control can suppress the disturbance generated by the GFM inverter by reducing the power coupling between the GFL inverter and the GFM inverter. To verify the effect of voltage-feedforward control, an unsatisfactory damping parameter value is selected, i.e., D_p = 0.4. Fig. 12 (a) and (b) show the power response of the hybrid inverters to external 5 Hz disturbance without the voltage-feedforward control for the GFL inverter, the ripple of P_e^{GFM} and Q_e^{GFM} has impact on P_e^{GFL} and Q_e^{GFL}, especially for Q_e^{GFL}. However, the effect of the GFM inverter can be reduced significantly with F_v^{GFL} = 1, as depicted in Fig. 12 (c) and (d). The response amplitude of P_e^{GFL} decreases from 70 W to 30 W, and 80 Var to 8 Var for Q_e^{GFL}. It can be explained as the application of voltage-feedforward control makes the GFM inverter is less sensitive to the variation of V_{PCC}, which achieves the decoupling of the GFM and the GFL inverter to a certain extent. Therefore, the voltage-feedforward control can be an easy way to enhance the stability of the GFL inverter in hybrid inverters.

B. Experimental Results

To verify the effectiveness of the proposed quantitation method, experimental tests were performed on a 2-kW GFM inverter and a 1.5 kW GFL inverter with the experimental platform in Fig. 13, and the circuit and control parameters are the same with TABLE I and II.

To validate the coupling characteristics of the hybrid inverters at different frequencies in the low-frequency range, a power disturbance of ΔX_d is added to the power command, being with $\Delta X_d = 0.05 P_{ref} \cdot \sin(2\pi f_d t)$ (X = P or Q for active

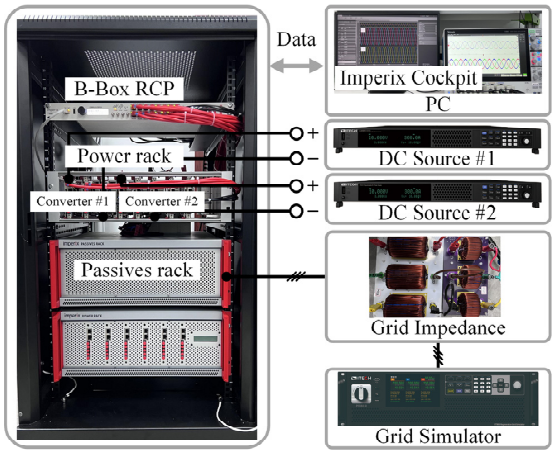

Fig. 13: Setup experimental of the hybrid inverters with a GFL inverter and a GFM inverter.

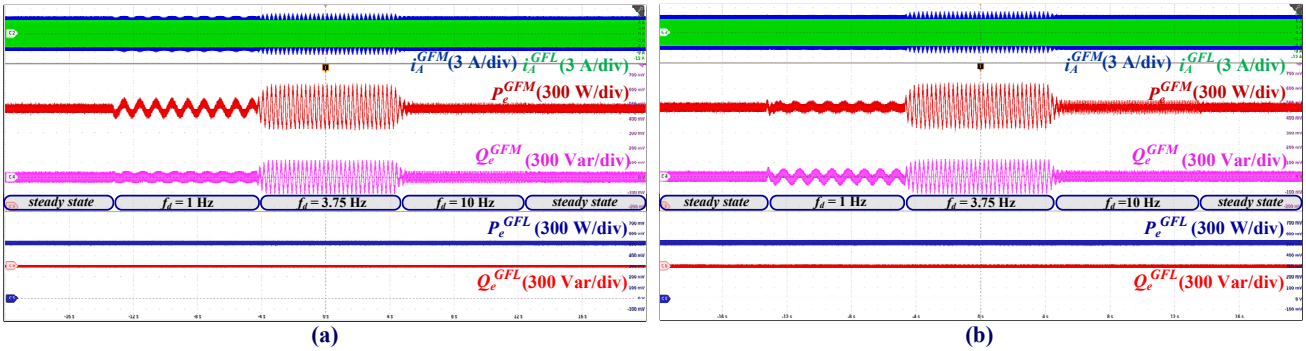

Fig. 14: Experimental results of the system in response to power disturbances; (a) disturbance in P_{ref}^{GFM} and (b) disturbance in Q_{ref}^{GFM}.

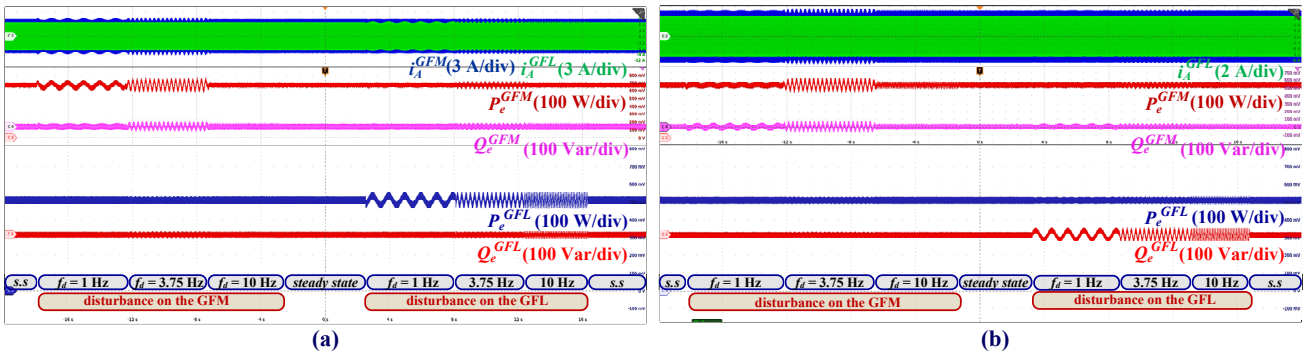

Fig. 15: Experimental results of the system in response to power disturbance, (a) disturbance in P_{ref}^{GFM} and P_{ref}^{GFL}, (b) disturbance in Q_{ref}^{GFM} and Q_{ref}^{GFL}, where s.s stands for steady state of the system.

power or reactive power respectively). As shown in Fig. 14, the GFM inverter is more sensitive to the disturbance with $f_d = 3.75$ Hz than other disturbance frequencies ($f_d = 1$ Hz and $f_d = 10$ Hz) under a strong grid (L_g = 1 mH), which agrees well with the quantitative analysis in Fig. 5. Under the same disturbance, the GFL inverter is hardly affected by the GFM inverter, as shown in Fig. 14.

Under a weak grid (L_g = 11 mH), the coupling between the GFL inverter and the GFM inverter is strong, as shown in Fig. 15, which shows the fluctuation of one of the output power (P_e^{GFL}, Q_e^{GFL}, P_e^{GFM}, and Q_e^{GFL}) of the hybrid inverters can affect others significantly. Comparing the experimental results of Fig. 15 (a) and (b), it can be seen that the disturbance with $f_d = 3.75$ Hz on the GFM inverter is more significant than other disturbances, while the influence of disturbances with different frequencies on the GFL inverter is almost the same. It indicates that the grid impedance increases the power coupling among the hybrid inverters, and the coupling characteristics of the GFL and GFM inverter are different in the low-frequency range.

V. Conclusion

This paper proposed a method to quantitatively analyze the coupling effect in a hybrid system with parallel GFL and GFM inverters. This paper also provides a detailed analysis process to apply this method to analyze the coupling between any specified control loops ($\mathbf{u} \rightarrow \mathbf{y}$) quantitatively. The coupling among power loops under different grid impedances, power commands, and control strategies is explored. It is indicated system configuration including the grid strength and the operating points significantly affect the power interaction between the GFL inverter and the GFM inverter, while the voltage-feedforward can improve the robustness of the GFL inverter against disturbances. The influence of control parameters, e.g., inertia coefficient J, damping coefficient D_p, and the voltage-feedforward control F_v^{GFL} are discussed. The analysis results are verified by the simulation and experimental tests.

References

[1] J. Rocabert, A. Luna, F. Blaabjerg, and P. Rodríguez, "Control of power converters in ac microgrids," *IEEE Trans. Power Electron.*, vol. 27, no. 11, pp. 4734–4749, 2012.

[2] F. Blaabjerg, Y. Yang, K. A. Kim, and J. Rodriguez, "Power electronics technology for large-scale renewable energy generation," *Proc. the IEEE*, vol. 111, no. 4, pp. 335–355, 2023.

[3] L. Harnefors, M. Schweizer, J. Kukkola, M. Routimo, M. Hinkkanen, and X. Wang, "Generic pll-based grid-forming control," *IEEE Trans. Power Electron.*, vol. 37, no. 2, pp. 1201–1204, 2022.

[4] H. Wu, X. Ruan, D. Yang, X. Chen, W. Zhao, Z. Lv, and Q.-C. Zhong, "Small-signal modeling and parameters design for virtual synchronous generators," *IEEE Trans. Ind. Electron.*, vol. 63, no. 7, pp. 4292–4303, 2016.

[5] A. Tayyebi, D. Groß, A. Anta, F. Kupzog, and F. Dörfler, "Frequency stability of synchronous machines and grid-forming power converters," *EEE J. Emerging Sel. Top. Power Electron.*, vol. 8, no. 2, pp. 1004–1018, 2020.

[6] B. He, W. Chen, X. Li, L. Shu, Z. Zou, and F. Liu, "Unified frequency-domain small-signal stability analysis for interconnected converter systems," *IEEE J. Emerging Sel. Top. Power Electron.*, vol. 11, no. 1, pp. 532–544, 2023.

[7] K. Shi, W. Song, H. Ge, P. Xu, Y. Yang, and F. Blaabjerg, "Transient analysis of microgrids with parallel synchronous generators and virtual synchronous generators," *IEEE Trans. Energy Convers.*, vol. 35, no. 1, pp. 95–105, 2020.

[8] Y. Wang, W. Wang, C. Wang, and X. Wu, "Coupling analysis on current control at low switching frequency for the three-phase pwm converter based on rga and a novel output feedback decoupling method," *IEEE Trans. Ind. Electron.*, vol. 63, no. 11, pp. 6684–6694, 2016.

[9] J. Jia, X. Yan, B. Qin, A. Siddique, and B. Zhang, "Extended two-terminal network model of parallel vsms for analysis of active power–frequency response," in *In Proc. of IEEE ECCE*, 2020, pp. 3231–3237.

[10] B. Qin, Y. Xu, C. Yuan, and J. Jia, "A unified method of frequency oscillation characteristic analysis for multi-vsg grid-connected system," *IEEE Trans. Power Delivery*, vol. 37, no. 1, pp. 279–289, 2022.

[11] X. Wang, X. Ruan, S. Liu, and C. K. Tse, "Full feedforward of grid voltage for grid-connected inverter with lcl filter to suppress current distortion due to grid voltage harmonics," *IEEE Trans. Power Electron.*, vol. 25, no. 12, pp. 3119–3127, 2010.

[12] Y. Gu and T. C. Green, "Power system stability with a high penetration of inverter-based resources," *Proc. IEEE*, vol. 111, no. 7, pp. 832–853, 2023.

[13] S. Liao, Y. Chen, M. Huang, X. Fu, X. Zha, L. Wang, A. Luo, and J. M. Guerrero, "Clustering-based modeling and interaction analysis of multiple differently parameterized grid-side inverters in pmsg wind turbines," *IEEE Trans. Energy Convers.*, vol. 36, no. 4, pp. 3031–3043, 2021.

[14] J. Beerten, S. D'Arco, and J. A. Suul, "Identification and small-signal analysis of interaction modes in vsc mtdc systems," *IEEE Trans. Power Delivery*, vol. 31, no. 2, pp. 888–897, 2016.

[15] W. M. F., "Interacting control systems : Steady state and dynamic measurement of interaction," *ISA Trans.*, vol. 16, pp. 35–41, 1977.

[16] Y. Wang, W. Wang, C. Wang, and X. Wu, "Coupling analysis on current control at low switching frequency for the three-phase pwm converter based on rga and a novel output feedback decoupling method," *IEEE Trans. Ind. Electron.*, vol. 63, no. 11, pp. 6684–6694, 2016.

[17] F. Wang, J. L. Duarte, M. A. M. Hendrix, and P. F. Ribeiro, "Modeling and analysis of grid harmonic distortion impact of aggregated dg inverters," *IEEE Trans. Power Electron.*, vol. 26, no. 3, pp. 786–797, 2011.

[18] R. K. Sharma, S. Mishra, and P. Barsaiyan, "Dynamic power coupling analysis of droop based autonomous microgrid using dynamic relative gain array," in *Proc. of PEDES*, 2020, pp. 1–6.

[19] X. Ji, D. Liu, K. Jiang, Z. Zhang, and Y. Yang, "Small-signal stability of hybrid inverters with grid-following and grid-forming controls," *Energies*, vol. 17, no. 7, 2024.

[20] Q. Zheng, F. Gao, Y. Li, Y. Zhu, and Y. Gu, "Equivalence of impedance participation analysis methods for hybrid ac/dc power systems," *IEEE Trans. Power Syst.*, vol. 39, no. 2, pp. 3560–3574, 2024.

[21] Y. Arkun, "Dynamic block relative gain and its connection with the performance and stability of decentralized control structures," *Int. J. Control*, vol. 46, no. 4, pp. 1187–1193, Oct. 1987.

[22] N. Pogaku, M. Prodanovic, and T. C. Green, "Modeling, analysis and testing of autonomous operation of an inverter-based microgrid," *IEEE Trans. Power Electron.*, vol. 22, no. 2, pp. 613–625, 2007.

[23] M. Chen, D. Zhou, and F. Blaabjerg, "Active power oscillation damping based on acceleration control in paralleled virtual synchronous generators system," *IEEE Trans. Power Electron.s*, vol. 36, no. 8, pp. 9501–9510, 2021.

[24] *Minimum Specification Required for Provision of GB Grid Forming (GBGF) Capability*, National Grid Electricity System Operator (ESO) Std.